JOURNAL OF COMPUTATIONAL PHYSICS 26, 87–106 (1978)

Pseudospectral Solution of Atmospheric Diffusion Problems

HANS WENGLE* AND JOHN H. SEINFELD

Department of Chemical Engineering, California Institute of Technology, Pasadena, California 91125

Received January 18, 1977

The pseudospectral method is applied to the solution of advection/diffusion problems arising from the dispersion of contaminants in the atmosphere. Two techniques are developed for the pseudospectral treatment of nonperiodic boundary conditions that typically exist in such problems. Calculations using the two forms of the pseudospectral method are presented for the dispersion of a contaminant emitted from an elevated, crosswind line source in the atmosphere. The results indicate that pseudospectral methods offer a promising alternative to finite-difference methods for such problems.

1. INTRODUCTION

The prediction of the dynamic behavior of trace contaminants in the atmosphere is generally approached through numerical solution of the so-called atmospheric diffusion equation [1,2],

$$\frac{\partial c}{\partial t} + u\frac{\partial c}{\partial x} + v\frac{\partial c}{\partial y} + w\frac{\partial c}{\partial z} = \frac{\partial}{\partial x}\left(K_{xx}\frac{\partial c}{\partial x}\right) + \frac{\partial}{\partial y}\left(K_{yy}\frac{\partial c}{\partial y}\right) + \frac{\partial}{\partial z}\left(K_{zz}\frac{\partial c}{\partial z}\right), \qquad (1)$$

where c is the mean concentration of the contaminant (assumed chemically inert); u, v, and w are the three components of the mean wind velocity; and K_{xx}, K_{yy}, and K_{zz} are the turbulent eddy diffusivities.

Considerable effort has been devoted to the study of the numerical solution of (1). By and large, these studies have been concerned with finite-difference methods, often with emphasis on reduction of the so-called numerical diffusion associated with the finite-difference approximation of the advective terms [3–9]. Finite-difference-solution methods have proved to be convenient, and there exists a large body of experience associated with the solution of advection/diffusion problems such as (1) by finite-difference methods. Relatively recently, however, a new class of numerical techniques, spectral and pseudospectral methods, has emerged that offers a promising alternative to finite-difference methods for the solution of partial differential equations. The application of spectral and pseudospectral methods has been particularly successful

* Present address: Lehrstuhl für Strömungsmechanik, Technische Universität, München, Munich, West Germany.

0021-9991/78/0261-0087$02.00/0

in the direct numerical solution of the two- and three-dimensional Navier–Stokes equations. Numerical simulations have been reported, for example, for two-dimensional, homogeneous turbulence [10–12], three-dimensional, homogeneous, isotropic turbulence [13], and inhomogeneous shear flows [14]. Other applications of the general spectral technique have been concerned with the equations of two- and three-dimensional guiding center plasmas [15], and Fourier expansion techniques have been used for the numerical solution of the Vlasov equation [16] and the solution of a class of linear second-order differential equations [17]. Of interest with respect to advection/diffusion problems such as (1) are the solutions for the two-dimensional advection of a scalar in a uniformly rotating flow field [18–20] and for the advective diffusion of a puff of material released by a line source in a two-dimensional shear flow [19].

In a spectral method the dependence of the dependent variable upon one or more of the independent variables (usually spatial variables) is represented by expansions in a discrete series of orthogonal functions. A Galerkin approach is used to project the original partial differential equation into a finite set of equations for the coefficients of the expansion. That is, the original partial differential equation is transformed into a set of ordinary differential equations relating the spectral coefficients of the fields of the independent variables so expanded. These equations contain convolution sums that arise from products of functions in physical space, sums that must be evaluated to solve the equations. An exact representation of all the retained frequencies is obtained, and neither phase errors nor aliasing terms are involved in the representation of spatial derivatives [20]. In a pseudospectral method the expansion of the dependent variable is used to evaluate directly, and without phase errors, the spatial derivatives. Products of functions are performed in physical space or wavenumber space, wherever the operations are local. Thereby, in a pseudospectral method the evaluation of convolution sums is avoided, but the resulting approximation contains aliasing terms [21]. In solving partial differential equations by spectral and pseudospectral methods very efficient computing schemes can be developed if Fourier series expansions are used. In such a case, the evaluation of convolution sums and of derivatives can be accomplished very efficiently by using a Fast-Fourier-Transform (FFT) algorithm [22].

The numerical solutions reported for advection/diffusion problems [18–20] show that the spectral and pseudospectral approaches produce more efficient computational schemes than conventional second- and fourth-order finite-difference methods. All the test problems previously considered [18–20] employed periodic boundary conditions. The numerical simulation of the dynamics of trace species in the atmosphere virtually always involves nonperiodic boundary conditions and, additionally, sources with constant or time-varying emission rates producing highly peaked and rapidly changing concentration distributions. The purpose of this paper is to apply the pseudospectral method to a two-dimensional version of (1) that retains all the relevant physical features of the full three-dimensional equation and that involves nonperiodic boundary conditions. In particular, we consider the advection and diffusion of a contaminant released by an elevated, infinite, crosswind line source into an atmospheric shear flow.

For theoretical aspects associated with pseudospectral methods we refer the reader to available literature [18, 20, 23–26]. (The main object of this work is to develop and test pseudospectral algorithms for the solution of atmospheric diffusion problems.) In Section 2 we develop in detail the treatment of nonperiodic boundary conditions using Chebyshev expansions or by decomposition of the spatial distribution of the dependent variable into periodic and analytical nonperiodic functions. In Section 3 we present the mathematical statement of the test problem, and in Section 4 we describe two different pseudospectral approximations for the numerical solution of the test problem based on different treatment of the nonperiodic boundary conditions. The two solution methods are implemented and compared in Section 5, where we also compare the results to available solutions by finite-difference and finite-element methods.

2. Treatment of Nonperiodic Boundary Conditions

We employ the pseudospectral method by using expansion of the dependent variable such that the coefficients of the expansion and the derivatives can be evaluated by an FFT algorithm. In addition, it is necessary that the expansions satisfy the boundary conditions.

Periodic boundary conditions can be satisfied naturally by using a Fourier series expansion for the dependent variable. If a periodic function $F(x)$ is specified by N values on equally spaced grid points $x_n = 2\pi n/N$, $n = 0, 1,..., N-1$, the corresponding values of the function $F_n \equiv F(x_n)$ may be expressed by a finite Fourier series expansion,

$$F_n = \sum_{|k| \leqslant N/2} f(k) \exp(ikx_n), \qquad n = 0, 1,..., N-1. \tag{2}$$

The Fourier coefficients $f(k)$ can be calculated by the corresponding inverse transform,

$$f(k) = \frac{1}{N} \sum_{n=0}^{N-1} F_n \exp(-ikx_n), \qquad |k| \leqslant N/2. \tag{3}$$

Differentiating expansion (2) term by term leads to an approximation for the derivatives $(\partial F/\partial x)_n$ at each x_n,

$$\left(\frac{\partial F}{\partial x}\right)_n = \sum_{|k| \leqslant N/2} [f(k)\, ik] \exp(ikx_n), \qquad n = 0, 1,..., N-1. \tag{4}$$

The accuracy of this approximation can be estimated from the convergence properties of Fourier expansion (2) [18, 27, 28]. The rate of convergence of the Fourier series depends on the degree ofsmoothness of $F(x)$, as measured by the order of the derivative that first becomes discontinuous at any point in the closed interval over which $F(x)$ is defined. Even if $F(x)$ is smooth at all orders of its derivatives within the interval, it may have discontinuities at the boundaries of the interval, and these discontinuities

will affect the rate of convergence of its Fourier series. If a periodic function $F(x)$ is infinitely differentiable, series (2) converges faster than any power of k^{-1} for $k \to \infty$, and the approximation is said to be of "infinite order." For functions having continuous derivatives only up to mth order, the coefficients in the Fourier series decrease as $k^{-(m+1)}$. A continuation of a real function $F(x)$ as an odd or even function (instead of a periodic continuation) outside of its original interval of definition, e.g., $[0, \pi]$, enables the satisfaction of boundary conditions like $F(0) = F(\pi) = 0$ or $\partial F/\partial x = 0$ ar $x = 0$ and π, thereby avoiding a decreased convergence rate of the Fourier expansion. In this case the proper expansions are Fourier sine or cosine series that can be evaluated very efficiently using a standard FFT subroutine for complex numbers with corresponding pre- and postprocessing routines for real even or odd data sets [29].

If the derivatives of nonperiodic functions are computed by a finite Fourier expansion, the series is slowly convergent due to the so-called "ringing" or Gibbs phenomenon at the discontinuities at the boundaries. In practical problems with nonperiodic boundary conditions it is necessary to improve the convergence rate of the expansions. In the present work we satisfy nonperiodic boundary conditions by two different procedures: (a) expanding $F(x)$ in Chebyshev polynomials, and (b) decomposing $F(x)$ into a third-order polynomial and a periodic residual.

2.1. *Chebyshev Polynomial Expansion*

The main advantage of using Chebyshev polynomial expansions is that the convergence rate depends only on the smoothness of the function that is approximated and not on the nature of the boundary conditions. In this case we have to specify $F(x)$ (e.g., on the interval $[-1, 1]$) by $(N + 1)$ values $F_n = F(x_n)$ at the grid points $x_n = \cos(\pi n/N)$, $n = 0, 1, \ldots, N$. With this choice the Chebyshev expansion is equivalent to a Fourier cosine expansion,

$$F_n = \sum_{k=0}^{N}{}'' a_k T_k(x_n) = \sum_{k=0}^{N}{}'' a_k \cos(\pi k n/N), \qquad n = 0, 1, \ldots, N, \tag{5}$$

where $T_k(\cdot)$ is the kth-degree Chebyshev polynomial defined by $T_k(\cos\theta) = \cos(k\theta)$. The double prime indicate that both the first and last terms of the sum are taken with a factor $\frac{1}{2}$. The coefficients a_k may be evaluated by the inverse transform of (5),

$$a_k = \frac{2}{N} \sum_{n=0}^{N}{}'' F_n \cos(\pi k n/N), \qquad |k| \leqslant N/2. \tag{6}$$

Applying the specific properties of the Chebyshev polynomials, we may evaluate an expansion for the derivatives with new coefficients $a_k^{(1)}$,

$$\frac{\partial F}{\partial x_n} = \sum_{k=0}^{N}{}'' a_k \frac{\partial T_k(x_n)}{\partial x} = \sum_{k=0}^{N}{}'' a_k^{(1)} T_k(x_n)$$

$$= \sum_{k=0}^{N}{}'' a_k^{(1)} \cos(\pi k n/N). \tag{7}$$

The coefficients $a_k^{(1)}$ may be calculated from the a_k using the recursive relation [28]

$$a_{k-1}^{(1)} = a_{k+1}^{(1)} + 2ka_k\,, \tag{8}$$

together with the starting conditions,

$$\begin{aligned} a_{N-1}^{(1)} &= 2Na_N\,, \\ a_{N-2}^{(1)} &= 2(N-1)\,a_{N-1}\,. \end{aligned} \tag{9}$$

Similar relations can be derived for higher-order derivatives. The coefficients a_k of (6) and the derivatives (7) can be evaluated by an FFT algorithm.

2.2. *Decomposition Procedure*

Since the discontinuities of a function $F(x)$, particularly those at the boundaries, control the convergence rate of a finite Fourier expansion, we may subtract certain functions, typically polynomials, from $F(x)$ so that the residual will appear to the FFT to be a periodic function with sufficiently continuous higher derivatives [27,30]. For example, we can represent $F(x)$ as

$$F(x) = F_p(x) + F_r(x), \tag{10}$$

where $F_p(x)$ and $F_r(x)$ are polynomial and periodic residual, respectively. The derivatives of $F(x)$ are

$$\begin{aligned} F'(x) &= F_p'(x) + F_r'(x), \\ F''(x) &= F_p''(x) + F_r''(x). \end{aligned} \tag{11}$$

In particular, in subsequent applications, we choose $F_p(x)$ as a third-order polynomial,

$$F_p(x) = F(0) + b_1x + b_2x^2 + b_3x^3, \tag{12}$$

with $F_p'(x) = b_1 + 2b_2x + 3b_3x^2$ and $F_p''(x) = 2b_2 + 6b_3x$. The periodicity of $F_r(x)$ requires that $F_r(0) = F_r(L)$, $F_r'(0) = F_r'(L)$, $F_r''(0) = F_r''(L)$, where the domain of interest is taken to be $[0, L]$. The coefficients b_1, b_2, and b_3 are found from the periodicity conditions as

$$\begin{aligned} b_1 &= (1/L)\,[F(L) - F(0)] - b_2L - b_3L^2, \\ b_2 &= (1/2L)\,[F'(L) - F'(0)] - \tfrac{3}{2}\,b_3L, \\ b_3 &= (1/6L)\,[F''(L) - F''(0)]. \end{aligned} \tag{13}$$

To evaluate b_1, b_2, and b_3 we first have to provide approximations for the first and second derivatives of $F(x)$ at the boundaries, for example by polynomial interpolation. If these approximations are good enough, $F_r(x)$ will be a "sufficiently continuous" periodic function, the derivatives of which can be evaluated by Fourier expansions such as (3) and (4). The derivatives F_p' and F_p'' are then computed with

b_1, b_2, and b_3, and finally F' and F'' are evaluated from (11). The whole purpose of this procedure is to increase the convergence rate of the Fourier expansions of $F_r(x)$ by avoiding the Gibbs phenomenon.

2.3. *Numerical Examples*

We now investigate the accuracy of computed derivatives applying FFT techniques For this purpose we use three simple analytical functions on a one-dimensional grid. We compare the accuracy of the results from the two procedures for the treatment of nonperiodic boundary conditions by evaluating the local relative errors, ϵ_{rel}, e.g., for the first derivative of a function $F(x)$: $\epsilon_{rel} = (F'_{analytical} - F'_{computed})/F'_{analytical}$.

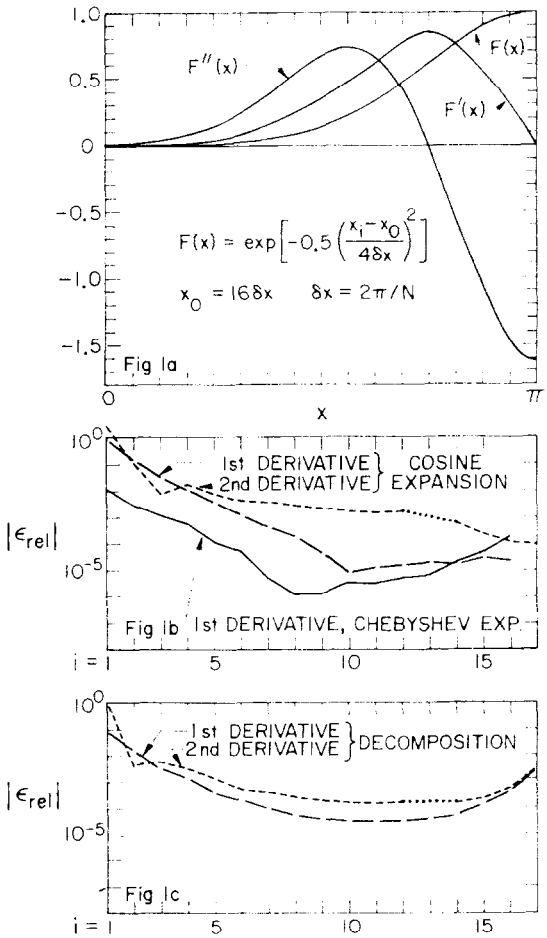

FIG. 1. Local relative errors of computed derivatives of a normal distribution (symmetrically located) using cosine and Chebyshev expansions (Fig. 1b) and a decomposition procedure (Fig. 1c) on a discrete grid with $(N + 1)$ grid points ($N = 16$).

For the first example, Fig. 1a, we use a normal distribution $F(x)$ located on a grid of $N + 1$ ($N = 16$) points such that an even continuation of the function outside the interval $[0, \pi]$ is possible. If we expand $F(x)$ in a Fourier cosine series, the first derivatives $F'(x)$ will be represented by a Fourier sine series and the second derivatives will be represented again by a Fourier cosine series. With these expansions, the computed first derivatives are exactly zero at the boundaries $x = 0$ and π. The corresponding local relative errors, $|\epsilon_{\text{rel}}|$, will then increase for $x \to 0$, (see Fig. 1b) since the analytical values for the first derivatives are approaching zero only for $x \to -\infty$. Applying a Chebyshev expansion of $F(x)$, instead, improves $|\epsilon_{\text{rel}}|$ by about two orders of magnitude (for the first derivative) in the region $x \to 0$, as seen in Fig. 1b. The decomposition procedure also produces very accurate first and second derivatives (see Fig. 1c) except at the left-hand-side boundary ($F'(0)$ and $F''(0)$), which indicates that the polynomial approximation of these values in the decomposition procedure was poor.

For the second example, shown in Fig. 2a, we use an exponential function that

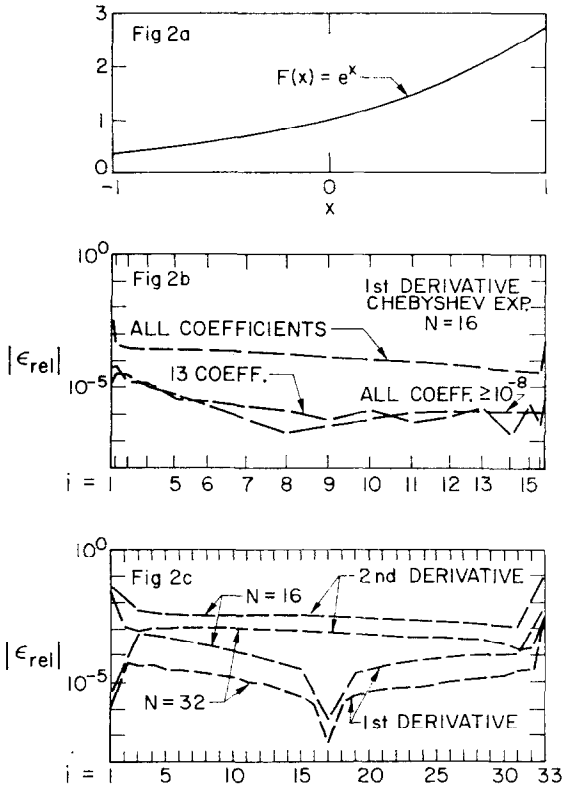

FIG. 2. Local relative errors of computed derivatives of an exponential function using a Chebyshev expansion (Fig. 2b) and a decomposition procedure (Fig. 2c) on a discrete grid with ($N + 1$) grid points ($N = 16$ and $N = 32$).

would cause the "ringing" phenomenon at the boundaries applying a finite Fourier expansion. Using a Chebyshev expansion instead, an average accuracy of $|\epsilon_{rel}| \approx 10^{-4}$ results for the first derivative over the whole interval (Fig. 2b). The recursive algorithm (8) for the computation of the new coefficients $a_k^{(1)}$ in the expansion for the first derivative $F'(x)$ by using the prior coefficients a_k in the expansion for the function $F(x)$ may be ill-conditioned in the sense that errors in the smallest coefficients are magnified and decrease the accuracy of even the largest $a_k^{(1)}$. This problem can be checked easily for the exponential function used in this example, since in this case $a_k^{(1)}$ should be equal to a_k. Terminating the sequence of coefficients $a_k^{(1)}$ after having decayed to a small value (e.g., 10^{-8}) or just ignoring the last two or three coefficients improves the accuracy of the first derivatives significantly, as shown in Fig. 2b. Figure 2c contains the local relative errors $|\epsilon_{rel}|$ for the computed first and second derivatives applying the decomposition procedure. Increasing the number of grid points, of course, improves the accuracy, but the least accuracy for the derivatives generally must be expected to be at the boundaries.

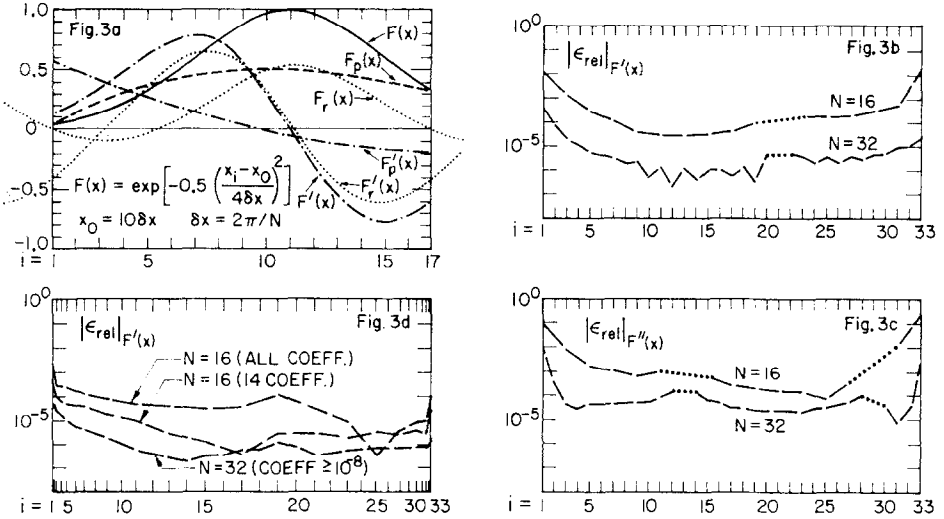

FIG. 3. Local relative errors of computed derivatives of a normal distribution (nonsymmetrically located) using a Chebyshev expansion (Fig. 3d) and a decomposition procedure (Figs. 3b and c) on a discrete grid with $(N + 1)$ grid points ($N = 16$ and $N = 32$).

In the third example we located the normal distribution from the first example nonsymmetrically. The results of the decomposition of $F(x)$ and its derivative $F'(x)$ into polynomials $F_p(x)$, and $F_p'(x)$ and periodic residuals $F_r(x)$, and $F_r'(x)$ are shown in Fig. 3a for $N = 16$. Figures 3b and c show the distribution of $|\epsilon_{rel}|$ for the computed first and second derivatives, respectively (for $N = 16$ and $N = 32$). Again, the most accurate derivatives result from a Chebyshev polynomial expansion (see Fig. 3d).

In summary, we find by computing the derivatives of three simple test functions using the two different procedures for the treatment of nonperiodic boundary conditions, that

(a) expanding the given smooth functions into a Chebyshev polynomial series always produced the most accurate results (as measured by the local relative error), and

(b) the accuracy of the decomposition procedure depends critically on the adequacy of the approximation of the derivatives at the boundaries of the interval.

3. Test Problem: Dispersion of a Contaminant from an Elevated, Crosswind Line Source

As a test problem we consider the dispersion of an inert contaminant from an elevated crosswind line source in the atmosphere. The line source of strength Q_0 is located at a height h above the ground at $x = 0$ and begins emitting at $t = 0$. The resultant plume is confined between the ground ($z = 0$) and an elevated stable layer at $z = H$. The mean concentration $c(x, z, t)$ is governed by the following special case of (1),

$$\frac{\partial c}{\partial t} + u(z)\frac{\partial c}{\partial x} = \frac{\partial}{\partial z}\left(K_{zz}\frac{\partial c}{\partial z}\right), \tag{14}$$

where the turbulent mass flux in the x-direction has been neglected relative to advection The initial condition is

$$c(x, z, 0) = 0. \tag{15}$$

The boundary conditions at $z = 0$ and H reflect the physical conditions of no contaminant fluxes across the two planes,

$$\frac{\partial c}{\partial z} = 0, \qquad z = 0, H. \tag{16}$$

Finally, the $x = 0$ boundary condition specifies the source condition,

$$c(0, z, t) = (Q_0/u(h))\,\delta(z - h). \tag{17}$$

This test problem contains all the relevant physical features of (1), namely wind shear and advection, vertical turbulent diffusion, and time variation.

Equations (14)–(17) may be placed in dimensionless form by defining $Z = z/H$, $X = xK_{zz}(H)/H^2u(H)$, $\tau = tK_{zz}(H)/H^2$, $U = u/u(H)$, $K = K_{zz}/K_{zz}(H)$, and $C = u(H)\,Hc/Q_0$. The result is

$$\frac{\partial C}{\partial \tau} + U(Z)\frac{\partial C}{\partial X} = \frac{\partial}{\partial Z}\left(K(Z)\frac{\partial C}{\partial Z}\right), \tag{18}$$

$$C(X, Z, 0) = 0, \tag{19}$$

$$C(0, Z, \tau) = \delta(Z - \Theta)/U(\Theta), \tag{20}$$

$$\partial C/\partial Z = 0, \qquad Z = 0, 1, \tag{21}$$

where $\Theta = h/H$, the dimensionless height of the source.

We will assume that the dimensionless velocity $U(Z)$ and eddy diffusivity $K(Z)$ are described by power-law distributions,

$$U(Z) = Z^{\alpha}, \tag{22}$$

$$K(Z) = Z. \tag{23}$$

The main reason for our choice forms (22) and (23) is that system (18)–(23) corresponds to that considered previously [7, 8, 31]. Thus, we will be able to compare our results to those obtained previously by these authors using other numerical techniques. Physically, a linear variation of K_{zz} with z is associated with neutral stability, in which case α would be close to $\frac{1}{7}$ in value. For the purpose of our numerical study will consider values of α ranging from 0 to 0.5.

The steady-state form of (18), subject to (20)–(23) has the exact solution [32]

$$C(X, Z) = (1 + \alpha) \sum_{j=0}^{\infty} \frac{J_0\{\beta_j Z^{(1+\alpha)/2}\}\, J_0\{\beta_j \Theta^{(1+\alpha)/2}\}}{J_0(\beta_j)^2} \exp\left[-\frac{(1 + \alpha)^2 \beta_j X}{4}\right], \tag{24}$$

where $J_0(\cdot)$ is the Bessel function of the first kind of order zero, and β_j are the roots of $J_1(\beta) = 0$. The steady-state solution will be useful in evaluating the numerical solution of (18) once C has achieved steady state.

4. Numerical Solutions by Pseudospectral Approximation

In this section we develop the procedures to solve the test problem of Section 3 based on the general discussion of Section 2. For the numerical solution of a two-dimensional problem we can select individual one-dimensional expansions in Z and X or a two-dimensional expansion in Z and X. In this work we have chosen the former. Computations with a two-dimensional Chebyshev–Cosine expansion showed no significant improvement in accuracy but required about 60% more computing time per time step.

4.1. *Use of Expansions in Chebyshev Polynomials and Fourier Cosine Series*

The boundary conditions (21) can be satisfied by expanding the vertical concentration distribution in a Fourier cosine series,

$$C(X, Z, \tau) = \sum_{k=0}^{K_2}{}'' \tilde{C}(k, \tau) \cos(\pi k Z), \qquad X = \text{constant}. \tag{25}$$

With an equidistant vertical grid point distribution $Z_j = j/K_2]$, $j = 0, 1, \ldots, K_2$, coefficients $\tilde{C}(k, \tau)$ may be evaluated by an inverse transform (FFT^{-1}) of (25),

$$\tilde{C}(k, \tau) = \frac{2}{K_2} \sum_{j=0}^{K_2}{}'' C(X, Z_j, \tau) \cos(\pi k j / K_2), \qquad X = \text{constant}. \tag{26}$$

Differentiating (25) term by term leads to expansions for $\partial C/\partial Z$ and $\partial^2 C/\partial Z^2$ that can be evaluated with an FFT subroutine using the coefficients from (26),

$$\left[\frac{\partial C}{\partial Z}\right]_j = \sum_{k=0}^{K_2}{}'' [-\tilde{C}(k, \tau)\, \pi k] \sin(\pi k j/K_2), \tag{27}$$

$$\left[\frac{\partial^2 C}{\partial Z^2}\right]_j = \sum_{k=0}^{K_2}{}'' [-\tilde{C}(k, \tau)(\pi k)^2] \cos(\pi k j/K_2), \tag{28}$$

where the subscript j indicates that the derivatives are evaluated at Z_j.

We expand the horizontal concentration distribution in (shifted) Chebyshev polynomials, and we use the nonequidistant sampling points, $X_i = L(1 - \cos(\pi i/K_1))/2$. The result is a Fourier cosine expansion for the horizontal concentration distribution,

$$C(X, Z, \tau) = \sum_{k=0}^{K_1}{}'' \tilde{C}(k, \tau)\, T_k\left(\frac{2X - L}{L}\right) = \sum_{k=0}^{K_1}{}'' \tilde{C}(k, \tau) \cos(\pi i k/K_1), \quad Z = \text{constant}. \tag{29}$$

The first derivatives again result by differentiating (29) term by term,

$$\left(\frac{\partial C}{\partial X}\right)_i = \sum_{k=0}^{K_1}{}'' \tilde{C}(k, \tau) \frac{\partial T_k}{\partial X} = \sum_{k=0}^{K_1}{}'' \tilde{C}^{(1)}(k, \tau)\, T_k\left(\frac{2X - L}{L}\right), \qquad Z = \text{constant}, \tag{30}$$

where the new coefficients $\tilde{C}^{(1)}(k, \tau)$ may be calculated from the old coefficients $\tilde{C}(k, \tau)$ by relations (8) and (9), replacing the factor 2 in these equations by a factor 4 (since we use shifted Chebyshev polynomials defined on [0, 1] instead of [−1, 1]).

The numerical solution of the advection–diffusion equation (18) proceeds in the following way (see the schematic outline labeled Method A in Fig. 4). At a particular time level n (where $\tau = n\,\Delta\tau$) we evaluated the coefficients of the expansion in the Z-direction (25) and in the X-direction (29) by inverse FFTs. The new Chebyshev coefficients $\tilde{C}^{(1)}(k, \tau)$ for the derivatives in the X-direction may be calculated using (8) and (9). The evaluation of the first and second derivatives (for the Z-direction) in the wavenumber space are local operations, and the derivatives in physical space at all grid points may be evaluated by FFTs (27), (28), and (30). Note that we decompose the eddy diffusion term $\partial(K\partial C/\partial Z)/\partial Z$ into the two terms $(\partial K/\partial Z)(\partial C/\partial Z)$ and $K\partial^2 C/\partial Z^2$, so that both terms can be evaluated by local operations in physical space. Finally, the advance to time level $n + 1$ is accomplished by a finite-difference step. We have chosen a second-order Adams–Bashforth predictor and Adams–Moulton corrector scheme which allowed a relatively large time step.

4.2. *Use of a Decomposition Procedure*

We now consider the other alternative for satisfying nonperiodic boundary conditions described in Section 2. At a particular time level n we decompose the concentration distribution separately in each direction into a third-order polynomial C_p

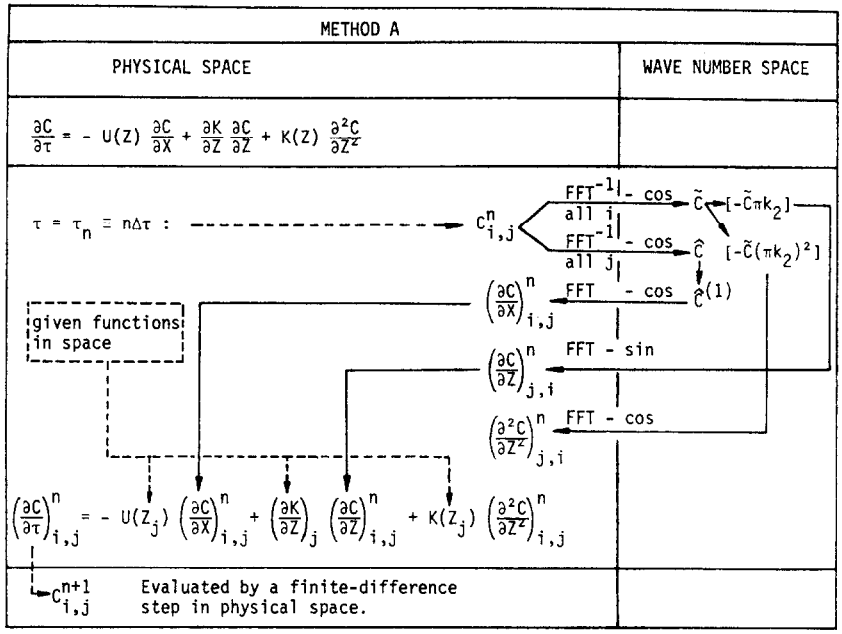

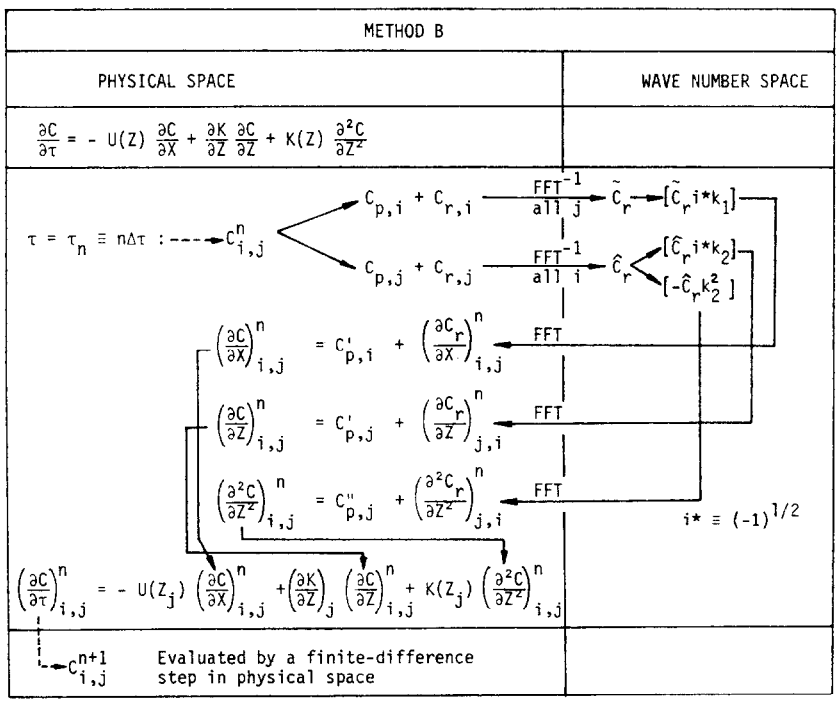

FIG. 4. Steps in the solution of the atmospheric diffusion equation by two different pseudo-spectral approximations.

and a periodic residual function C_r. For example, in the X-direction (individually at all levels $j = 0, 1,..., K_2$) the decomposition is

$$C(X_l, Z_j, \tau) = C_p(X_l, Z_j, \tau) + C_r(X_l, Z_j, \tau), \qquad l = 0, 1,..., K_1. \tag{31}$$

If we provide approximations for the first and second derivatives of C at the boundaries $X = 0$ and L, the coefficients b_1, b_2, and b_3 for the polynomial C_p can be evaluated by (13). (Note that L is just the arbitrary extent of the X-domain.) Thereby, the values of C_p and its derivatives at all grid points can be determined. Subtracting the polynomials C_p from the concentration distribution gives the periodic residual function C_r that may be expanded in a Fourier series to evaluate its derivatives using FFTs. At all levels $j = 0, 1,..., K_2$ we have

$$\begin{aligned} C_r(X_l, Z_j, \tau) &= C(X_l, Z_j, \tau) - C_p(X_l, Z_j, \tau) \\ &= \sum_{|k| \leqslant K_1/2} \tilde{C}_r(k, \tau) \exp(ikX_l), \qquad l = 0, 1,..., K_1 - 1. \end{aligned} \tag{32}$$

Also,

$$\left(\frac{\partial C_r}{\partial X}\right)_l = \sum_{|k| \leqslant K_1/2} [\tilde{C}_r(k, \tau)\, ik] \exp(ikX_l), \qquad l = 0, 1,..., K_1 - 1. \tag{33}$$

We apply the same procedure in the Z-direction to provide all the desired derivatives at the grid points. In Fig. 4 we present a schematic outline of this method, referred to in Fig. 4 as Method B. Only the derivatives of the periodic residual functions are computed by FFT techniques, the derivatives of the third-order polynomials may be calculated analytically by using approximations (polynomial interpolation) of the derivatives of the concentration field at its boundaries.

5. Discussion of Numerical Results

The test problem (18)–(23) has been solved using the pseudospectral Methods A and B described in Section 4 for the following set of parameters: $\Theta = 0.2$; $\alpha = 0$, 0.2, and 0.5; $L = 0.2$. The value of $L = 0.2$ ensures that advection and turbulent diffusion produce a nearly uniform vertical distribution of material at $X = L$. The exponents $\alpha = 0$, 0.2, 0.5 are characteristic of a uniform flow field, a moderately sheared field, and a strongly sheared field, respectively.

The grid for the the two pseudospectral methods was $K_1 = K_2 = 20$ with a constant dimensionless time step of $\Delta\tau = 10^{-3}$. To represent the Dirac delta function in (20) we computed a value of C at the source location by assyming a uniform concentration distribution over one-half a grid distance above and below the source,

$$\begin{aligned} C(0, Z, \tau) &= \frac{1}{U(\Theta)\,\Delta Z}, \qquad \Theta - \frac{\Delta Z}{2} < Z < \Theta + \frac{\Delta Z}{2}, \\ &= 0 \qquad\qquad \text{elsewhere.} \end{aligned} \tag{34}$$

To compute concentration values at $Z = 0$, where $U = 0$ (for $\alpha > 0$), $\partial C/\partial Z = 0$, and $K = 0$, it is necessary to extrapolate the interior concentration distribution or to evaluate U and K at a point Z_0, $0 < Z_0 < \Delta Z$.

We consider first the case of a uniform flow field, $\alpha = 0$. In this case a sharp concentration front moves away from the source with speed $U = 1$, and steady-state conditions are established immediately behind the location of the front as it passes a given point. This case is a useful one for studying numerical solutions, as the representation of the sharp concentration front is a particularly severe test of any numerical method. Figure 5 shows the computed concentrations at the source

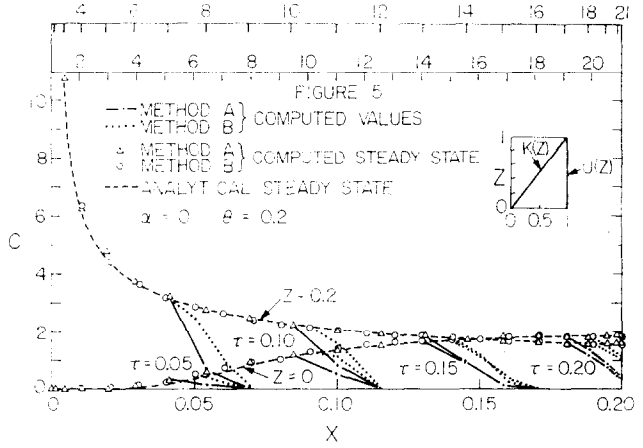

FIG. 5. Time-dependent concentration distributions for $\alpha = 0$ at source height ($Z = \Theta = 0.2$) and at the ground ($Z = 0$).

height ($Z = \Theta = 0.2$) and at ground level ($Z = 0$) at times $\tau = 0.05$, 0.10, 0.15, 0.20, and 0.25 for the two methods. At the last time ($\tau = 0.25$) steady-state conditions prevail throughout the entire field. At these times the concentration front should be at $X = 0.05$, 0.10, 0.15, 0.20, and 0.25, correspondingly. The pseudospectral solutions in Fig. 5 indicate that the method is capable of producing a relatively sharp front moving with the correct speed, even though for Method A the grid points in the X-direction are nonequidistantly distributed at $X_i = 0.5L \times 1 + \cos(\pi i/K_1))$. The computed steady-state results can be compared to the analytical solution (24), and it can be seen from Fig. 5 that both methods produce very accurate steady-state concentration profiles.

The second case considered is that of $\alpha = 0.2$, a wind profile roughly characteristic of neutrally stable conditions. In Fig. 6 we compare computed concentration profiles at $Z = 0.2$ and $Z = 0$ by both methods. Because of the interaction of wind shear and vertical turbulent diffusion the concentration front is smoothed out and moves with different speeds at different heights. The approach of the concentrations to steady state at different locations is shown in Fig. 7. In Fig. 7 we show the computed concentrations at two locations at source height very close to the source, a

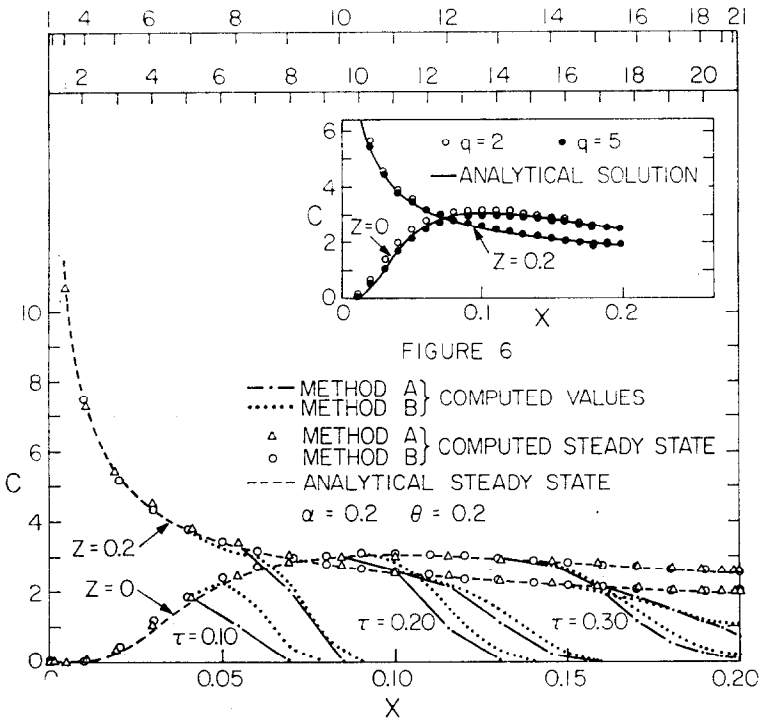

FIG. 6. Time-dependent concentration distribution for $\alpha = 0.2$ at source height ($Z = \Theta = 0.2$) and at the ground ($Z = 0$). The inset shows the results of Runca and Sarei [7].

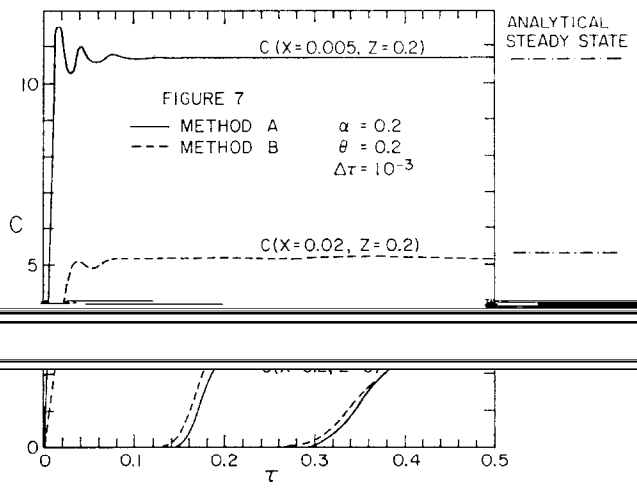

FIG. 7. Time-dependent concentration values for $\alpha = 0.2$ at several locations.

location in the middle of the field at the ground, and the location ($X = 0, 2, Z = 0$) which is the last one to attain steady state. The corresponding steady-state values from the analytical solution (24) are shown at the right-hand side of the figure. The pseudospectral methods give a characteristic oscillatory behavior in time very close to the source. However, after a short initial period these oscillations disappear. In Fig. 8 we compare the computed steady-state vertical concentration profiles at different X locations to the analytical solution (24). Both methods produce highly accurate steady-state solutions. The steady-state solutions obtained here are somewhat more accurate than those of Runca and Sardei [7] reproduced in the inset to Fig. 8 that were obtained by a mixed Eulerian–Lagrangian method.

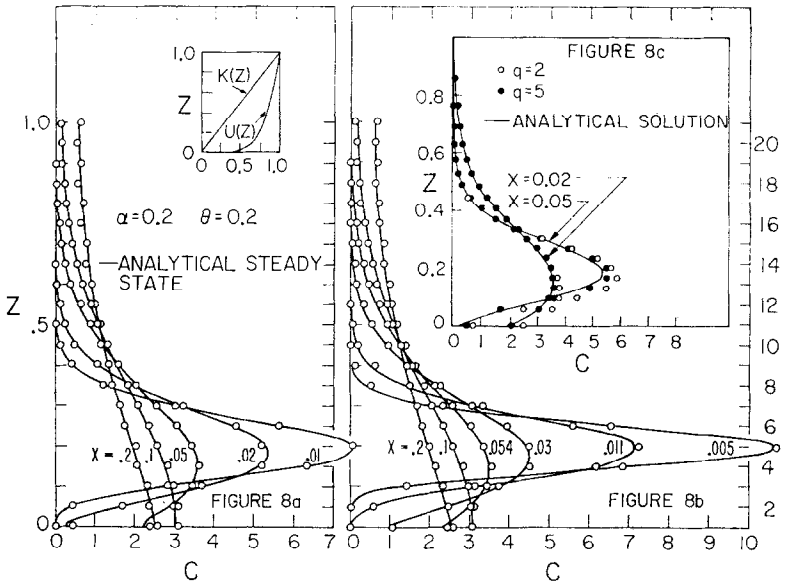

FIG. 8. Steady-state vertical concentration distributions for $\alpha = 0.2$ as computed by Method A (Fig. 8b) and Method B (Fig. 8a). The inset (Fig. 8c) shows the results from Runca and Sardei [7].

The third case, $\alpha = 0.5$, is characterized by a strongly sheared wind field and significant interaction between wind shear and vertical turbulent diffusion. A rapid accumulation of material at the ground close to the source takes place in this case. Steady-state conditions are first reached at levels above the source, whereas more time is required for the concentrations close to the ground to achieve steady state. Figure 9 shows the concentration distributions at $Z = 0$, calculated by both methods at different times $\tau = 0.10, 0.20, 0.40$ and 0.60. There is excellent agreement between the two methods concerning the time behavior of the concentration field. For the steady state, reached at about $\tau = 1.0$, Method B gives the more accurate results. Figure 10 shows selected vertical steady-state concentration distributions. The pseudospectral profiles are very accurate in the regions of high concentration and

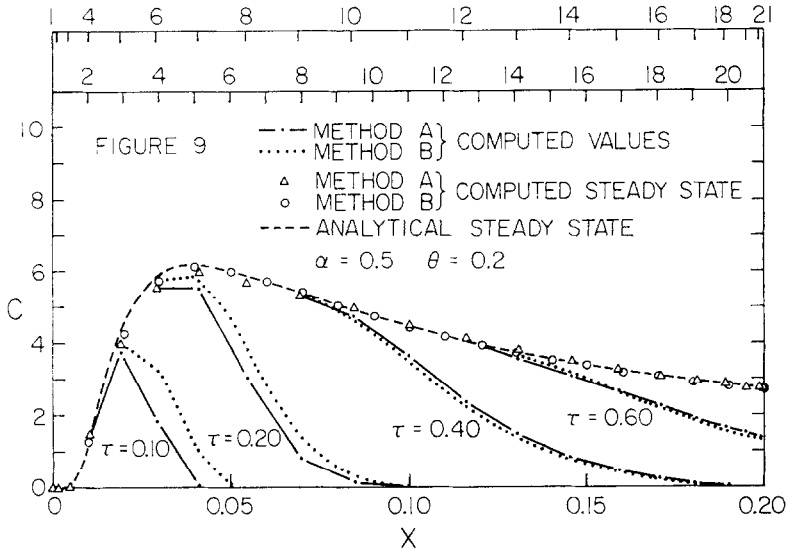

FIG. 9. Time-dependent concentration distributions for $\alpha = 0.5$ at the ground ($Z = 0$).

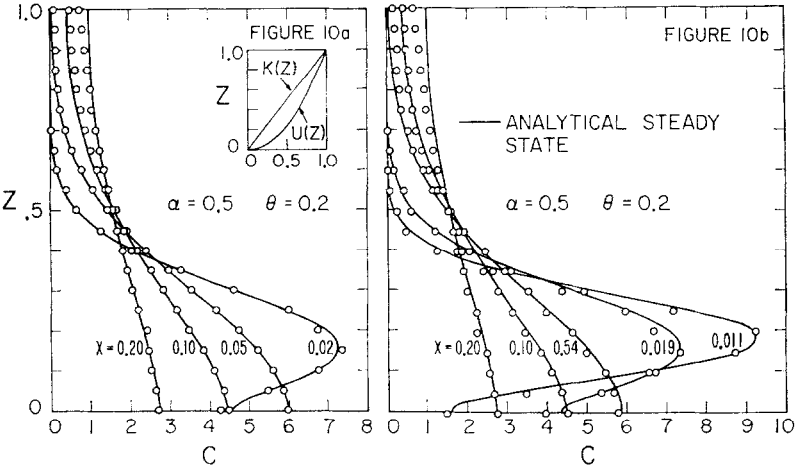

FIG. 10. Steady-state vertical concentration distributions for $\alpha = 0.5$ as computed by Method A (Fig. 10b) and Method B (Fig. 10a).

exhibit discrepancies only close to $Z = 1.0$. The advection-dominated peaks are reproduced extremely well; however, the methods have less success with the "diffusion-dominated" boundary condition $\partial C/\partial Z = 0$ at $Z = 1$. On the whole, however, the accuracy for the steady-state profiles predicted by both pseudospectral approximations in all three cases ($\alpha = 0$, 0.2, 0.5) is very satisfying.

The major problem in applying a pseudospectral method for the numerical solution of the test problem was the oscillatory spatial errors in the solution, typical for a method using Fourier expansions. In the highly peaked field close to the source these errors cause oscillating positive and negative concentration values at the outer edges of the concentration distribution where the errors finally reach the same order of magnitude as the concentration values. To eliminate disturbances in the downstream concentration field we defined the concentrations to be zero in regions where the information content of the data was completely dominated by these oscillating errors. The use of a predictor–corrector time step also improved significantly the time behavior of the system. We have chosen a second-order Adams–Bashforth predictor and Adams–Moulton corrector scheme.

The same test problem considered here has been solved numerically by a mixed Eulerian–Lagrangian finite-difference scheme [7], five different standard finite-difference schemes [8], and a finite-element method [31]. In Figs. 6 and 8 we included corresponding steady-state results from Runca and Sardei [7]. Unfortunately, for the case $\alpha = 0.5$ only three-dimensional plots at a single time ($\tau = 0.0224$) were given by Sardei and Runca [8], and these plots are not amenable to comparison with our results since no numerical values were provided in the figures. Finite-element results are available for the steady-state concentrations of the case $\alpha = 0.2$ (vertical distributions at $X = 0.02$ and 0.05; horizontal distributions at $Z = 0$ and 0.2) and for the vertical distribution at $X = 0.02$ for $\alpha = 0.5$ [31]. We chose not to show these profiles here. In general, the results obtained in the present study for the steady-state distributions ar somewhat more accurate than those reported in the other studies just cited.

In the choice of a particular method the main consideration is the accuracy attainable for a given computation time. The time-consuming aspect of a pseudospectral method is the repeated use of an FFT subroutine. All the computations reported here were carried out on a CDC 7600 computer at the Lawrence Berkeley Laboratory of the University of California. The programs were compiled in an optimized version by the FTN4-compiler (option 2). The approximate computation time for each method was 11 sec for 250 time steps ($\tau = 0.25$). Additional savings in computation time can be achieved by using an FFT subroutine in Assembler language rather than in Fortran. Direct comparisons of accuracy with the other methods used to solve the test problem were not possible although we were able to give some indication of the solutions obtained by other investigators in Figs. 6 and 8. The five finite-difference methods studied by Sardei and Runca [8] required between 36 and 42 sec on an IBM 360/91 for the case of $\alpha = 0.5$ and $\tau = 0.13$. If we assume that an IBM 360/91 is roughly two times slower than a CDC 7600 and that a finite-difference method requires twice as fine a spatial resolution as a pseudospectral method for a comparable level of accuracy, these finite-difference methods would require about three times more computation time than a pseudospectral method for comparable accuracy.

6. Concluding Remarks

We have demonstrated the feasibility of solving advection/diffusion problems, particularly those arising from atmospheric diffusion, by pseudospectral methods. The pseudospectral method is based on the principle of representing the dependent variable by an expansion in orthogonal functions to evaluate the spatial derivative very accurately at the zeros of the basic functions. The method is equivalent to an orthogonal collocation method with the particularity of applying expansions that enable the use of Fast-Fourier-Transform algorithms in passing back and forth between physical space and wavenumber space. The pseudospectral method is highly flexible and allows the inclusion of knowledge of the nature of the solution through the choice of the orthogonal functions and the choice of the particular space in which the calculations are to be carred out. Pseudospectral methods offer a promising alternative to finite-difference methods for the solution of atmospheric diffusion problems.

Acknowledgment

Hans Wengle was supported by a research grant from the Deutsche Forschungsgemeinschaft.

References

1. F. Pasquill, "Atmospheric Diffusion," Van Nostrand, New York, 1962.
2. A. S. Monin and A. M. Yaglom, "Statistical Fluid Mechanics", M.I.T. Press, Cambridge, Mass., 1971.
3. D. Randerson, *Atmos. Environ.* **4** (1970), 615.
4. B. A. Egan and J. R. Mahony, *J. Appl. Meteorol.* **11** (1972), 312.
5. C. C. Shir, *IBM J. Res. Develop.* **16** (1972), 171.
6. S. D. Reynolds, P. M. Roth, and J. H. Seinfeld, *Atmos. Environ.* **7** (1973), 1033.
7. E. Runca and F. Sardei, *Atmos. Environ.* **9** (1975), 69.
8. F. Sardei and E. Runca, An efficient numerical scheme for solving time dependent problems of air pollution advection and diffusion, *in* "Proceedings of the Seminar on Air Pollution Modeling, Nov. 27–28, 1975," Technical Report No. 48, IBM Venice Scientific Center, Italy.
9. E. Runca, An efficient air quality *K*-model, 7th International Technical Meeting on Air Pollution Modeling and Its Application, Sept. 7–10, 1976, Airlie, Va.
10. D. G. Fox and S. A. Orszag, *J. Computational Phys.* **11** (1973), 612.
11. J. R. Herring, S. A. Orszag, R. H. Kraichman, and D. G. Fox, *J. Fluid Mech.* **66** (1974), 417.
12. B. Fornberg, *J. Computational Phys.* **25** (1977), 1.
13. S. A. Orszag and G. S. Patterson, Jr., *Phys. Rev. Lett.* **28** (1972), 76.
14. S. A. Orszag and Y. Pao, *Advan. Geophys.* **18A** (1974), 225.
15. Y. Salu and G. Knorr, *J. Computational Phys.* **17** (1975), 68.
16. J. Gazdag, *J. Computational Phys.* **19** (1975), 77.
17. R. C. Le Bail, *J. Computational Phys.* **9** (1972), 440.
18. B. Fornberg, *SIAM J. Numer. Anal.* **12** (1975), 502.
19. A. Bass and S. A. Orszag, "Spectral Modeling of Atmospheric Flows and Turbulent Diffusion," EPA Report No. EPA-600/4-76-007, 1976.

20. S. A. ORSZAG, *J. Fluid Mech.* **49** (1971), 75.
21. S. A. ORSZAG, *Stud. Appl. Math.* **51** (1972), 253.
22. E. O. BRIGHAM, "The Fast Fourier Transform," Prentice–Hall, Englewood Cliffs, N.J., 1974.
23. S. A. ORSZAG AND M. ISRAELI, *Annu. Rev. Fluid Mech.* **6** (1974), 281.
24. S. A. ORSZAG, *Stud. Appl. Math.* **50** (1971), 293.
25. H. O. KREISS AND J. OLIGER, *Tellus* **24** (1972), 199.
26. J. GAZDAG, *J. Computational Phys.* **13** (1973), 100.
27. R. W. HAMMING, "Numerical Methods for Scientists and Engineers," 2nd ed., McGraw–Hill, New York, 1973.
28. L. FOX AND I. B. PARKER (1968), "Chebyshev Polynomials in Numerical Analysis," Oxford Univ. Press, New York, 1968.
29. J. W. COOLEY, P. A. W. LEWIS, AND P. D. WELCH, *J. Sound Vib.* **12** (1970), 315.
30. P. J. ROACHE, "Recent Developments and Problem Areas in Computational Fluid Dynamics" Lecture Notes in Mathematics, No. 46/7, Springer–Verlag, Berlin, 1975.
31. P. MELLI, An application of the Galerkin method to the Eulerian–Lagrangian treatment of time dependent advection and diffusion of air pollutants, *in* "Proceedings of the International Conference of Finite Elements for Water Resources, July 12–16, Princeton, 1976."
32. W. ROUNDS, *Trans. Amer. Geophys. Union* **36** (1955), 395.